The Role of the Circulation Patterns in Projected Changes in Spring and Summer Precipitation Extremes in the U.S. Midwest

Liang Chen[a,b], Trent W. Ford,[a] and Erik Swenson[c]

[a] Climate and Atmospheric Sciences Section, Illinois State Water Survey, Prairie Research Institute,
University of Illinois Urbana–Champaign, Champaign, Illinois
[b] Department of Earth and Atmospheric Sciences, University of Nebraska–Lincoln, Lincoln, Nebraska
[c] Center for Ocean–Land–Atmosphere Studies, George Mason University, Fairfax, Virginia

ABSTRACT: Recent studies suggest springtime wet extremes and summertime dry extremes will occur more frequently in the U.S. Midwest, potentially leading to devastating agricultural consequences. To understand the role of circulation patterns in the projected changes in seasonal precipitation extremes, the *k*-means clustering approach is applied to the large-ensemble experiments of Community Earth System Model, version 2 (CESM2-LE), and ensemble projections of CMIP6. We identify two key atmospheric circulation patterns that are associated with the extremely wet spring and extremely dry summer in the U.S. Midwest. The springtime wet extremes are typically linked to baroclinic waves with a northward shift of the North American westerly jet and positive anomalies in sea level pressure over the western Atlantic, which favor the development of the Great Plains low-level jet. The summertime dry extremes are associated with the development of an anomalous ridge with suppressed storm tracks over the central United States. The projected increase in springtime wet extremes and summertime dry extremes can be attributed to significantly more frequent occurrences of the associated atmospheric regimes. Particularly, the intensity of wet extremes is expected to increase mainly due to the enhanced moisture flux from the Gulf of Mexico. The moisture budget analysis suggests that the precipitation extremes are mainly associated with the dynamic component of atmospheric circulation. CESM2-LE and CMIP6 exhibit good agreement in the projected changes in circulation patterns and precipitation extremes. Our results explain the mechanism of the projected changes in the Midwest seasonal precipitation and highlight the contribution of circulation patterns to hydroclimatic extremes.

KEYWORDS: Extreme events; Precipitation; Climate models; Ensembles; Clustering

1. Introduction

Precipitation extremes, such as heavy precipitation and drought, can result in significant environmental impacts on water resources and ecosystems, and socioeconomic impact on agriculture, transportation, and industry. Particularly, variations of warm-season precipitation extremes may lead to devastating consequences in agricultural production in the U.S. Midwest, which is one of the most intense agricultural areas in the world. For instance, the 2012 drought resulted in widespread failure of corn, sorghum, and soybean crops, with an estimated loss of $36.9 billion (NOAA 2022). Meanwhile, extremely wet springs can limit corn and soybean yields in the Midwest (Urban et al. 2015), and the impacts of excessive rainfall on crop yields can be equivalent to those caused by extreme droughts (Li et al. 2019). Several studies have demonstrated significant socioeconomic impacts of seasonal precipitation variability and precipitation extremes in the Midwest, including water quality (Loecke et al. 2017), native flora and fauna (Swanston et al. 2018; Magee et al. 2019), and stormwater management (Moore et al. 2016).

Global climate change is expected to increase atmospheric moisture and affect the hydrological cycle (O'Gorman and Schneider 2009), resulting in the changes in frequency and intensity of precipitation extremes (both heavy precipitation and drought). Observations have shown significant increasing trends in heavy precipitation in the Midwest during the warm season over the past decades (Kunkel et al. 2020; Li et al. 2022). Climate projections also suggest significant increases in extreme precipitation intensity and frequency in spring by the end of the century (Chen and Ford 2021). Although the historical change in droughts over the Midwest is not as evident as heavy precipitation extremes, future projections suggest an increasing trend in some metrics of dry extremes, such as consecutive dry days (Akinsanola et al. 2020), and warm-season extreme drought risks (Cook et al. 2020). However, it is important to understand the mechanisms driving precipitation extremes and how global climate change affects these extremes through large-scale atmospheric circulation. Indeed, confidence or uncertainty in such projections of future precipitation changes is partly informed by the models' capability to represent synoptic-scale circulation patterns associated with such extremes. However, relatively few studies have evaluated projected changes in the atmospheric drivers of precipitation extremes.

Using the *k*-means clustering approach, Zhang and Villarini (2019) found that up to 40% of precipitation in the Midwest can be associated with a zonally aligned wave train propagating from the North Pacific to North America, which leads to

strong moisture flux transport from the Gulf of Mexico to the Midwest. A similar mechanism of heavy precipitation is also confirmed by a deep learning approach (Davenport and Diffenbaugh 2021), which suggests increased frequency and intensity of extreme precipitation over the past two decades. Recent studies (Chen and Ford 2023; Zhou et al. 2022) find that there are likely to be significantly intensified wet and dry extremes across the Midwest by the end of the century, with more frequent transitions from an extremely wet spring to an extremely dry summer. In Zhou et al. (2022), the wetter spring is linked to the enhanced Great Plains low-level jet (GPLLJ) (and consequently inland moisture transport) while the drier summer is linked to the weakened storm track (and consequently weakened synoptic disturbance). Both the enhanced springtime GPLLJ and the summertime weakened storm tracks are further linked to the poleward shift of the North American westerly jet. However, the relationship between the wet/dry extremes and synoptic-scale circulation patterns and how climate change affects the synoptic-scale circulation patterns are not well understood.

To fill the knowledge gap discussed above, in this study, we will use the k-means clustering analysis and large-ensemble climate experiments to examine the relationship between large-scale circulation patterns and precipitation extremes in the Midwest. We aim to address two research questions: 1) What circulation patterns are related to the Midwest springtime wet extremes and summertime dry extremes? 2) How are those patterns expected to change in a warming climate?

2. Data and method

a. Large-ensemble experiments

Large-ensemble experiments are designed to separate forced response from internal variability of the climate system in the past and future evolution (Kay et al. 2015; Milinski et al. 2020). The mean of a large ensemble can sufficiently eliminate the noise of internal variability (e.g., ENSO), which has considerable impacts on global precipitation, and can be used as an estimator for the forced response (Frankcombe et al. 2018). Therefore, to sufficiently understand the effects of external forcing [e.g., greenhouse gas (GHG)-induced global warming], we use the large ensemble of Community Earth System Model, version 2 (CEMS2-LE). CESM2 is the latest generation of the coupled Earth system model developed as collaborative efforts among the National Center for Atmospheric Research (NCAR), universities, and other research institutions, and contains significant improvements compared to its predecessor CESM1 (Danabasoglu et al. 2020). It also contributes to phase 6 of the Coupled Model Intercomparison Project (CMIP6).

The CESM2-LE experiments consist of 100 ensemble members produced with CESM2. Initial conditions of the 100 ensemble members include a mix of macro- and microperturbations, in which macroinitializations have one member for each initialization year (with a total of 20 initialization years) and microinitializations have twenty members applied with a small random perturbation for each initialization year (with a total of 4 initialization years).

Meanwhile, both the macro- and microperturbations use two different forcing fields to represent the variability of biomass burning (Rodgers et al. 2021). Due to the data availability of the CESM2-LE from NCAR's Climate Data Gateway, 79 ensemble members are used in our analysis. Daily output of total precipitation and 500-hPa geopotential height (Z500) are provided for the period 1850–2100 following the historical and shared socioeconomic pathway (SSP) SSP370 forcing protocols with a spatial resolution of 1.25° in longitude and 0.9° in latitude, and 32 vertical levels with the top level at 2.26 hPa. The output during the period 1981–2100 is used in our analysis. More details of the CESM2-LE experiments can be found in Rodgers et al. (2021).

b. CMIP6

To examine the uncertainty related to the choice of model, we also use the historical and future SSP370 simulations from eight climate models in CMIP6, shown in Table S1. The eight models are used because they provide daily output of precipitation and Z500 in both the historical and SSP370 periods. Although multiple ensemble members are available for some models, to maintain the consistency among the models, only their first ensemble member is used in our analysis.

c. Reanalysis datasets

To evaluate the performance of CESM2-LE, we compare the ensemble mean of CESM2-LE with two reanalysis datasets: ERA5 (Hersbach et al. 2020) from the European Centre for Medium-Range Weather Forecasts (ECMWF) and the Modern-Era Retrospective Analysis for Research and Applications, version 2 (MERRA-2; Gelaro et al. 2017), from the Global Modeling and Assimilation Office (GMAO) at NASA. The evaluation is conducted for the period 1981–2014. Those two reanalysis datasets have been used to investigate the connection between meteorological phenomena (e.g., heatwaves, droughts, and heavy precipitation) and large-scale circulation patterns in recent studies (Agel and Barlow 2020; Gibson et al. 2017; Mastrantonas et al. 2021; Thomas et al. 2021). For comparison, results from ERA5 and MERRA-2 are regridded to the spatial resolution of CESM2-LE.

d. Identifying circulation patterns

According to previous studies (Chen and Ford 2023; Zhou et al. 2022), CMIP6 models show more frequent wet extremes in spring (March–May) and dry extremes in summer (July–September) by the end of the century, which is also confirmed by the CESM2-LE projections (shown in Fig. S1). Therefore, we first use composite analysis to explore the large-scale circulation patterns that are related to extremely wet spring and extremely dry summer. Following the method in Chen and Ford (2023), we identify extremely wet springs and extremely dry summers based on the 30-day standardized precipitation index (SPI). If any 30-day SPI during spring (MAM) is above 1.6, that spring is considered extremely wet; if any 30-day SPI during summer (JAS) is below −1.6, that summer is considered extremely dry. We focus on the mid- and late summer (JAS) because both CMIP6 and CESM2-LE suggest significantly
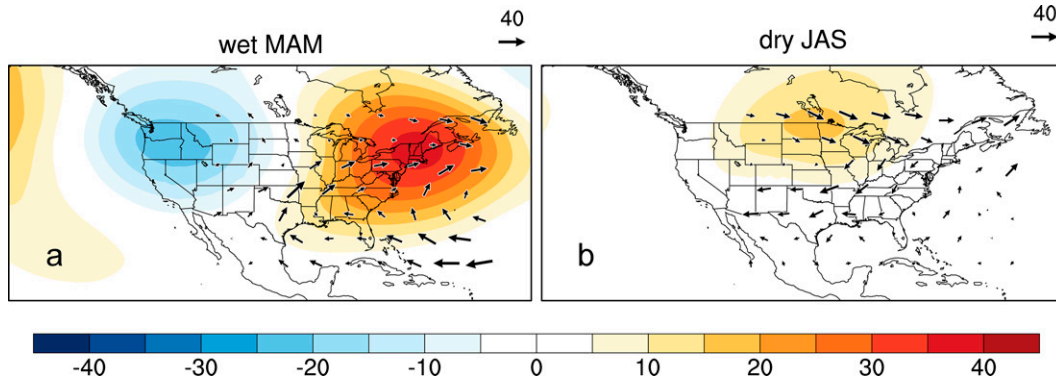
FIG. 1. Seasonal average of Z500 anomalies (m, shading) and vertically integrated moisture flux (kg m^{-1} s^{-1}, vectors only shown over the eastern United States) in (a) extreme wet springs and (b) extreme dry summers during 1981–2014. The extreme wet springs and extreme dry summers are identified based on the 30-day SPI.

more frequent dry extremes in those months (Fig. S1, and Chen and Ford 2023). We use the 30-day SPI as an indicator of wetness and dryness in spring and summer instead of the full 3-month seasonal SPI because precipitation extremes—both wet and dry extremes—at subseasonal time scales can induce significant agricultural and ecological impacts, even if they are embedded in a season with near-normal precipitation. For example, Westcott et al. (2005) showed Midwest corn yields were particularly sensitive to the subseasonal timing of 1-month wet and dry extremes in the spring and summer.

Meanwhile, atmospheric circulation patterns are classified through the k-means clustering method (Hartigan and Wong 1979), which is applied to daily Z500 anomalies from each ensemble member of CESM2-LE (for the period 1981–2100) and two reanalysis products (for the period 1981–2014). For a given calendar day, we detrend the Z500 time series using a cubic spline detrending method so that the nonlinear trends of thermodynamic warming in the troposphere can be removed. Figure S2 gives an example of the raw and detrended Z500 time series from an ensemble member of CESM2-LE. It should be noted that the detrending is done by removing the calendar trend in the regional average Z500 over a certain domain (Jézéquel et al. 2018; Agel et al. 2021; Chen et al. 2021; Davenport and Diffenbaugh 2021). This allows us to remove the uniform thermal dilation caused by tropospheric warming but preserve circulation patterns. For spring, the domain covers the continental United States (10°–50°N, 140°–60°W), and it is also used by Zhang and Villarini (2019). Considering the spatial pattern of Z500 anomalies during the Midwestern extreme dry summer (Fig. 1), the domain during summer covers the majority of the United States (30°–50°N, 115°–80°W).

The k-means clustering method is then applied to the detrended daily Z500 for those two domains in the spring (MAM) and summer (JAS) months, respectively. The k-means method is a centroid-based unsupervised clustering method and has been commonly used to classify synoptic patterns (Straus 2019; Zhang and Villarini 2019; Chen et al. 2021; Agel et al. 2021). The algorithm starts with k randomly selected initial seeds for k clusters. Each sample is classified into a cluster based on the nearest Euclidean distance to the cluster centroid,

and the centroid is then recalculated. The process is repeated with a maximum of 100 iterations until the sum of variances within the cluster reaches a minimum. The number of clusters ($k = 5$) is determined based on a previous study (Zhang and Villarini 2019). We have tested other numbers of clusters. Four clusters are too few and six clusters do not generate more patterns. The maximum number of iterations is chosen based on Chen et al. (2021), and our sensitivity analysis suggests that more iterations do not affect the classification results (not shown). It should be noted that k-means clustering is an unsupervised machine learning algorithm, so its results from some ensemble members can be inconsistent with the identified clusters from other ensemble members. For instance, Fig. S3 shows the clusters from two ensemble members. The first ensemble (cmip6.f09_g17.LE2-1001.001) represents the patterns from the majority of the ensemble members of CESM2-LE, but some clusters in the second ensemble (cmip6.f09_g17.LE2-1251.008) do not have consistent patterns with other ensemble members. Therefore, those ensemble members (5 out of 79) are not used in our analysis. Nevertheless, the high level of reproducibility in the cluster patterns demonstrates their significance.

e. Vertically integrated moisture flux

To understand how moisture transport is associated with large-scale circulation patterns, we calculate daily vertically integrated moisture flux (MF), which is defined as

$$\mathrm{MF}_u = -\frac{1}{g} \int_{1000\mathrm{hPa}}^{300\mathrm{hPa}} qu\, dp, \tag{1}$$

$$\mathrm{MF}_v = -\frac{1}{g} \int_{1000\mathrm{hPa}}^{300\mathrm{hPa}} qv\, dp, \quad \text{and} \tag{2}$$

$$\mathrm{MF} = \sqrt{\mathrm{MF}_u^2 + \mathrm{MF}_v^2}, \tag{3}$$

where MF_u and MF_u represent the moisture flux in the zonal and meridional directions (in units of kg m^{-1} s^{-1}), respectively; u and v represent wind speed in the zonal and meridional directions; p is the pressure level; and g is the gravitational constant.
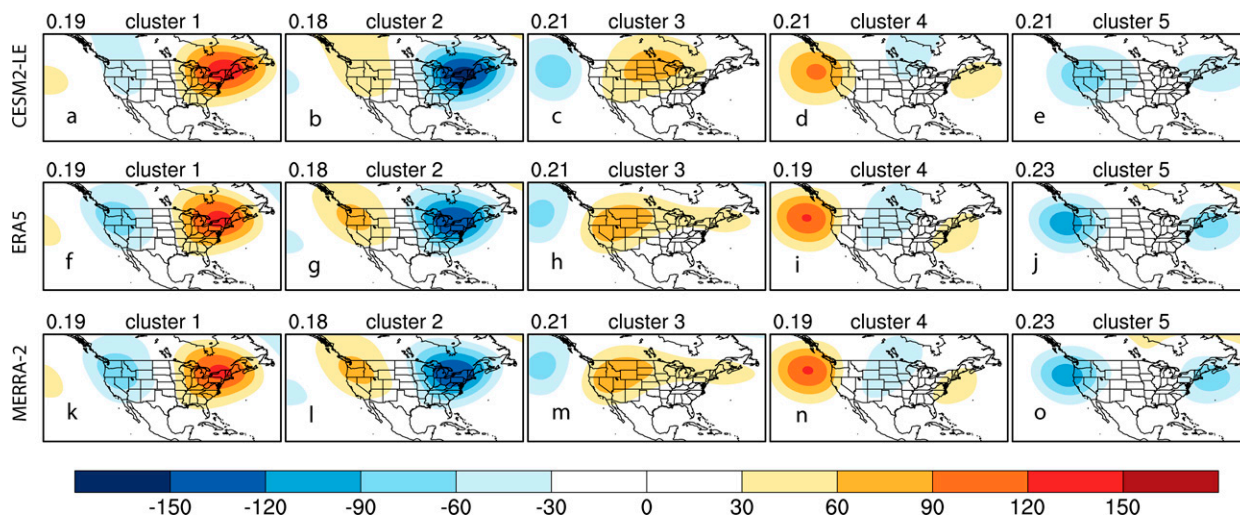
FIG. 2. Five springtime (MAM) circulation patterns identified using k-means clustering based on Z500 anomalies (m) during 1981–2014 in (a)–(e) CESM2-LE, (f)–(j) ERA5, and (k)–(o) MERRA-2. The frequency of each cluster is shown at the top-left corner of each panel.

f. Vertically integrated water budget

To further investigate the large-scale contributions to precipitation anomalies in the Midwest, we conduct a moisture budget analysis using the vertically integrated moisture budget equation:

$$P = E - \omega \frac{\partial q}{\partial p} - \mathbf{V} \cdot \nabla q - \frac{\partial q}{\partial t}, \qquad (4)$$

where P is precipitation, E is evapotranspiration, ω is vertical velocity, q is specific humidity, $\mathbf{V}$ is horizontal vector wind, and the brackets denote the mass integration through 100 hPa (Seager and Vecchi 2010; Cao et al. 2019; Hernandez and Chen 2022). The second and third terms on the right side of the equation represent the vertical and horizontal moisture advection, respectively. The fourth term, the time derivative of q, corresponds to the change in the atmospheric moisture storage, which is usually negligible and can be ignored (Sudharsan et al. 2020).

The variability of moisture budget can be further decomposed into

$$(P - E)' = -\omega' \frac{\partial \overline{q}}{\partial p} - \overline{\omega} \frac{\partial q'}{\partial p} - \mathbf{V} \cdot \nabla q', \qquad (5)$$

where the overbar denotes the monthly climatological value for the period 1981–2010, and the prime denotes the departure from the climatology. The first and second terms on the right side of Eq. (5) represent the dynamic and thermodynamic components of the vertical moisture advection, respectively (Chou and Lan 2012). The calculation of moisture budget is based on daily output from CESM2-LE, and all the terms in Eqs. (4) and (5) have units of millimeters per day.

g. NAWJ and storm tracks

According to Zhou et al. (2021, 2022), the projected changes in precipitation over the U.S. Midwest can be associated with the shift of the North American westerly jet (NAWJ) and changes in storm tracks. Here we use 500-hPa zonal wind as an NAWJ indicator. Storm tracks are estimated based on 850-hPa meridional wind v850, which is filtered using a fourth-order Butterworth bandpass filter with a 3–15-day cutoff period to only retain power at a synoptic time scale (Lutsko et al. 2019). The filtered meridional wind squared (vv850) is used to measure the storm-track intensity (Feng et al. 2019).

3. Seasonal circulation patterns

Figure 1 shows the seasonal mean Z500 anomalies in extremely wet springs and extremely dry summers. During extremely wet springs, the seasonal average Z500 is characterized by a ridge (positive anomalies) over the eastern United States and a trough (negative anomalies) over the western United States with strong moisture transport from the south to the Midwest (Fig. 1a), which is consistent with the spatial pattern of Z500 anomalies associated with precipitation extremes in previous studies (Zhang and Villarini 2019; Davenport and Diffenbaugh 2021). During extremely dry summers, there are positive Z500 anomalies over central North America (Fig. 1b), a pattern that is commonly associated with historical droughts with limited moisture flux in this region (Schubert et al. 2004; Hoerling et al. 2014).

4. Identified clusters during 1981–2014

To evaluate the performance of CESM2-LE, the k-means clustering method is applied to the detrended daily Z500 from CESM2-LE, ERA5, and MERRA-2. Figure 2 shows the five springtime circulation patterns and corresponding precipitation anomalies from the three datasets for the period 1981–2014. Overall, the ensemble mean of CESM2-LE shows a good agreement in the spatial pattern and magnitude of the identified circulation patterns. The pattern correlation (r) between the two reanalysis datasets is above 0.99; while the pattern
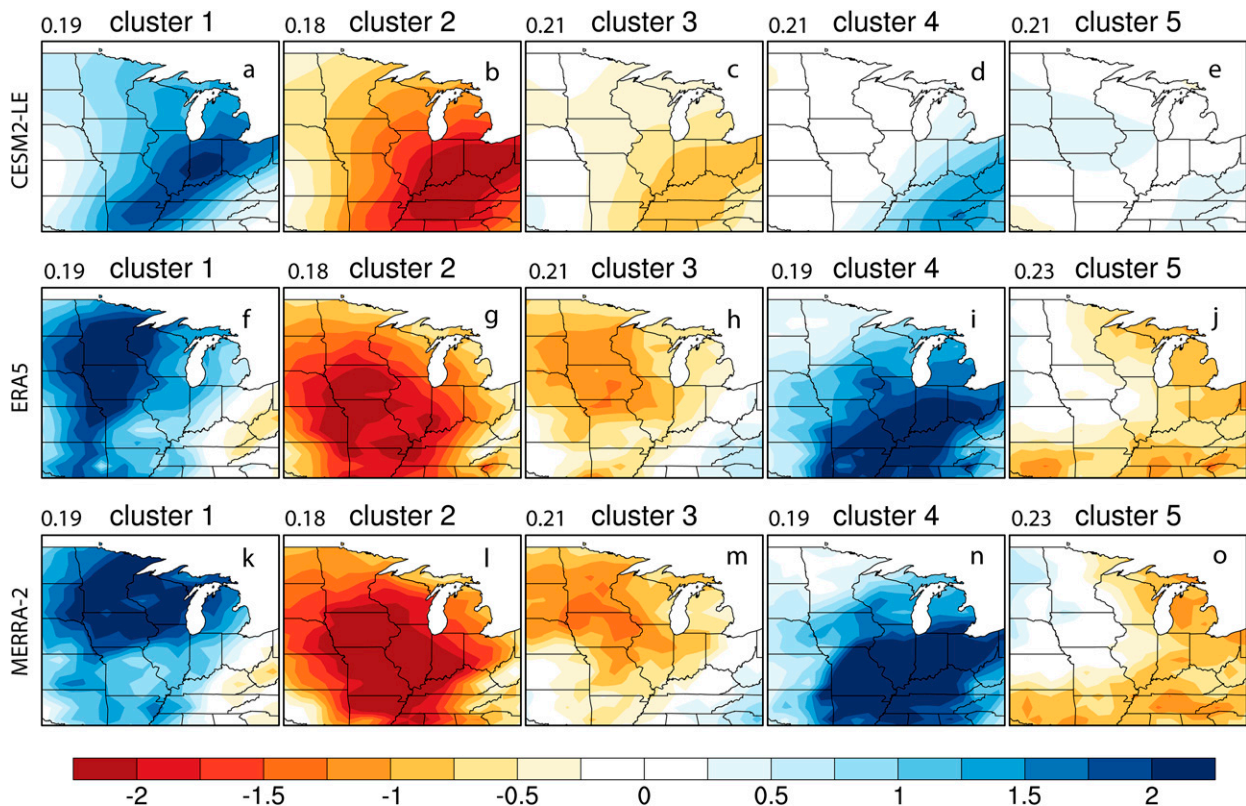
FIG. 3. Precipitation anomalies (mm day^{-1}) associated with the springtime circulation patterns during 1981–2014 in (a)–(e) CESM2-LE, (f)–(j) ERA5, and (k)–(o) MERRA-2. The frequency of each cluster is shown at the top-left corner of each panel.

correlation between CESM2-LE and ERA5/MERRA-2 is 0.71–0.92 ($r = 0.92$ for cluster 1 MAM). Cluster 1 MAM shows strong positive anomalies in Z500 over the eastern United States and relatively weak negative anomalies in the western United States, which is consistent with the Z500 anomalies during the Midwest's extreme wet springs (Fig. 1a). This "zonal wave train" pattern is also identified in previous studies (Zhang and Villarini 2019; Davenport and Diffenbaugh 2021), and is associated with strong positive precipitation anomalies in the Midwest (Fig. 3a).

Cluster 2 MAM shows an opposite pattern to cluster 1 MAM—strong negative anomalies in Z500 over the eastern United States and relatively weak positive anomalies in the western United States—and is associated with strong dry anomalies in the Midwest. Cluster 3 MAM is characterized by general positive anomalies over the United States. However, CESM2-LE shows stronger anomalies over the central United States, while ERA5 and MERRA-2 show stronger anomalies over the western United States. The positive Z500 anomalies correspond to overall dry anomalies in the Midwest. Cluster 4 MAM shows positive Z500 anomalies over the East Coast and West Coast, and cluster 5 MAM shows negative anomalies over the coasts. Consequently, these two patterns are associated with negative and positive precipitation anomalies in the eastern Midwest, respectively.

It should be noted that discrepancies exist in the corresponding precipitation anomalies among the three datasets.

For instance, CESM2-LE underestimates the wet anomalies in cluster 1 MAM, mainly because the large-ensemble mean has smoothed the variability. Also, there is less agreement in spatial patterns of the precipitation anomalies between CESM2-LE and reanalyses (or between ERA5 and MERRA-2) compared with the Z500 anomalies. Nevertheless, CESM2-LE can well capture the five springtime synoptic patterns identified in ERA5 and MERRA-2. Cluster 1 MAM is closely associated with extreme wet springs and will be the focus of our following analysis. Although cluster 4 MAM also corresponds to higher precipitation (particularly over the southeastern Midwest), its spatial pattern and magnitude do not well agree with the Z500 anomalies in extremely wet springs (Fig. 1a), and the wet anomalies are not evident in most areas of the Midwest according to CESM2-LE.

Five circulation patterns and associated precipitation anomalies in summer (JAS) are shown in Figs. 4 and 5. CESM2-LE well captures the spatial pattern and magnitude of the identified patterns. The pattern correlation between the two reanalysis datasets for each cluster is above 0.98; while the average pattern correlation between CESM2-LE and ERA5/MERRA-2 is 0.84–0.95 ($r = 0.95$ for cluster 1). Cluster 1 JAS is characterized by strong positive anomalies over the north-central United States and Canada and is associated with dry anomalies in the Midwest (Fig. 5a). This pattern is also found in the Z500 anomalies during the Midwest's extremely dry summers
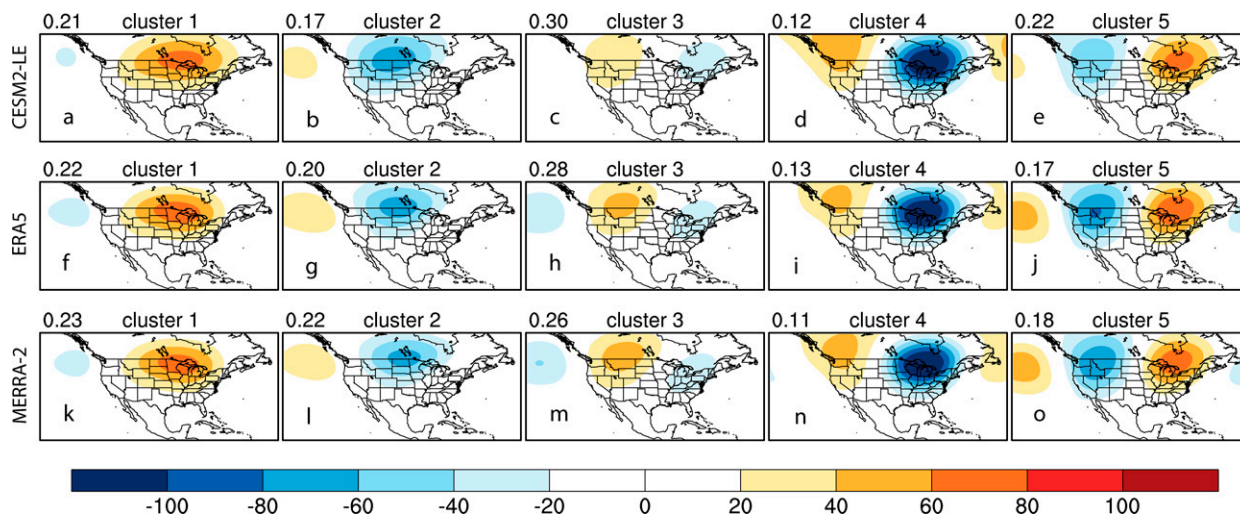
FIG. 4. Five summertime (JAS) circulation patterns identified using *k*-means clustering based on Z500 anomalies (m) during 1981–2014 in (a)–(e) CESM2-LE, (f)–(j) ERA5, and (k)–(o) MERRA-2. The frequency of each cluster is shown at the top-left corner of each panel.

(Fig. 1b). It should be noted that the orders of the patterns in Figs. 2 and 4 are not consistent. Cluster 1 MAM and cluster 1 JAS represent the springtime wet extremes and summertime dry extremes, respectively, because they are the two atmospheric patterns we are most interested in in this study (being consistent with Fig. 1). Accordingly, both cluster 2 MAM and cluster 2 JAS represent the opposite conditions.

Cluster 2 JAS is an opposite pattern to cluster 1 JAS. It shows negative Z500 anomalies in the north-central United States and Canada, consequently, corresponding to more precipitation over the Midwest. Cluster 4 JAS shows a strong low pressure system over the Great Lakes regions and positive anomalies over the Pacific Northwest. We find a mix of dry anomalies in the northwestern Midwest and wet anomalies in
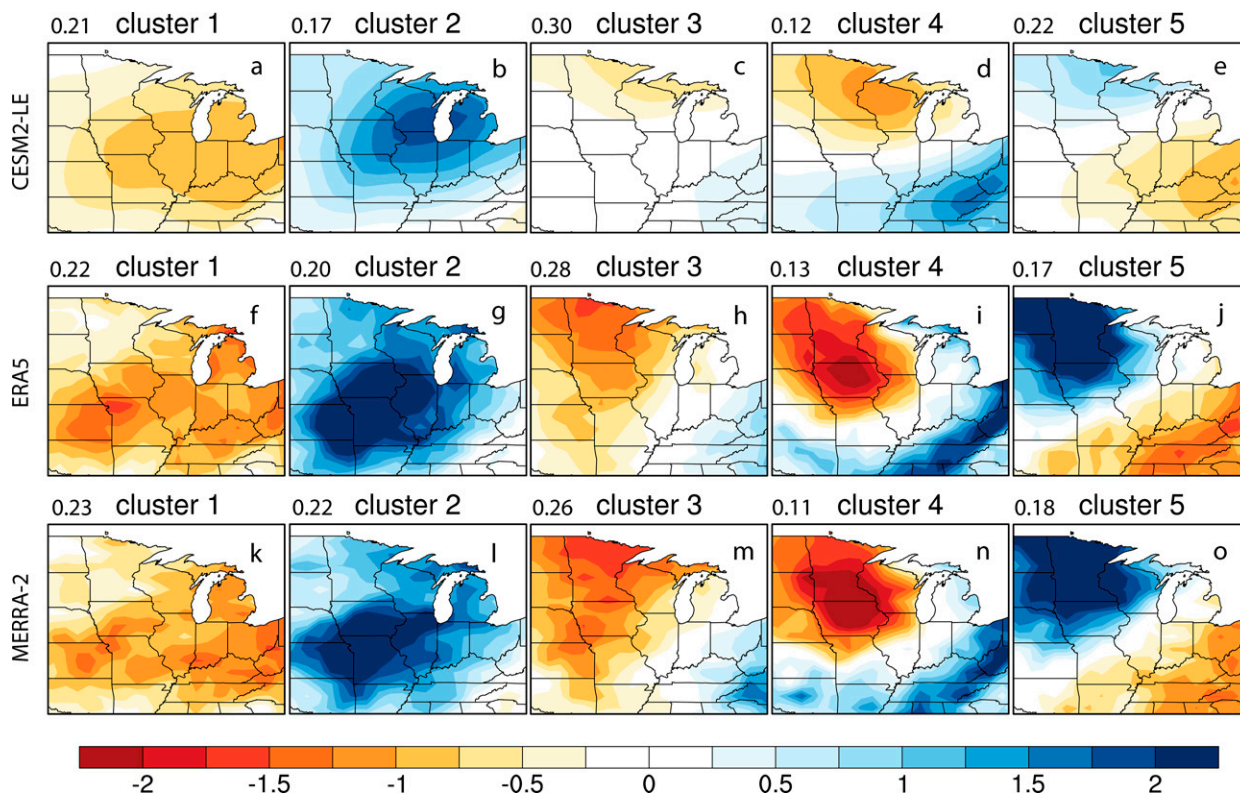

FIG. 5. Precipitation anomalies (mm day^{-1}) associated with the summertime circulation patterns during 1981–2014 in (a)–(e) CESM2-LE, (f)–(j) ERA5, and (k)–(o) MERRA-2. The frequency of each cluster is shown at the top-left corner of each panel.
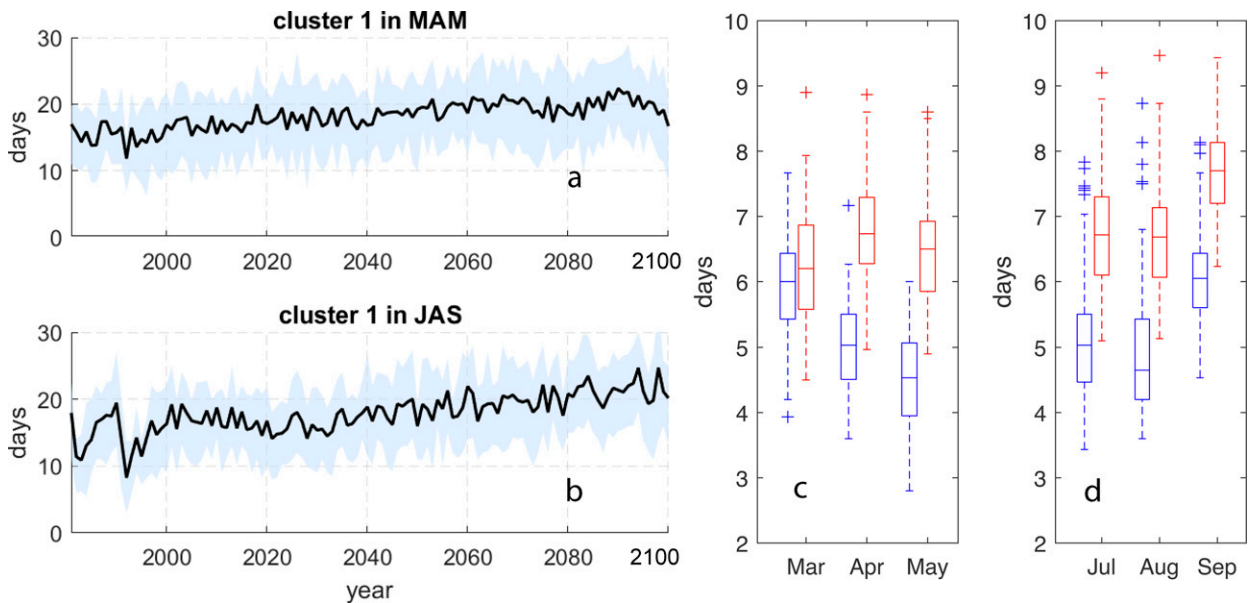
FIG. 6. Time series of frequency (days) of cluster 1 in (a) MAM and (b) JAS based on CESM2-LE during the period 1981–2100, and box plots of frequency (days) cluster 1 in individual (c) spring and (d) summer months. Shading in (a) and (b) shows the 25th–75th -percentile range. In (c) and (d), the blue boxes are based on the historical period 1981–2010, and red boxes are based on the SSP370 period 2071–2100.

the southeastern Midwest in the three datasets. Clusters 3 JAS and 5 JAS are generally two opposite patterns, with opposite anomalies over the eastern and western United States. Again, we see a good agreement in the circulation patterns between CESM2-LE and reanalyses, and cluster 1 JAS is identified as the synoptic pattern that is closely related to the summer dry extremes.

5. Projected changes in the identified patterns

From the analysis of circulation patterns and associated precipitation anomalies in the historical period, we identify two patterns or clusters that were consistently associated with wet spring extremes and dry summer extremes, respectively, and find a good agreement between CESM2-LE and ERA5/ MERRA-2. Therefore, we focus our analysis on the projected changes of these two patterns and their associated precipitation anomalies.

Figure 6 shows the time series of frequency of cluster 1 in spring and summer since 1981. Both clusters show a gradual increase, indicating more frequent wet extremes in spring and more frequent dry extremes in summer are expected under a warming climate. The increase rate is 0.4 ± 0.2 days decade^{-1} for cluster 1 in spring, and 0.6 ± 0.1 days decade^{-1} in summer. When scrutinizing the frequency in different months (Figs. 6c,d), the frequency of springtime cluster 1 shows significant increases in April and May, and summertime cluster 1 becomes more frequent in all three months (July, August, and September).

Meanwhile, we examine the projected changes in precipitation anomalies associated with the wet/dry clusters in spring and summer (Fig. 7). The wet anomalies in spring and dry anomalies in summer are projected to get stronger over the

Great Lakes regions, indicating that springtime wet extremes and summertime dry extremes can possibly get more intense. We also see the wet anomalies in summer are getting stronger (Fig. 7d), but with no significant changes in dry anomalies in spring (Fig. 7b). Additionally, we examine the projected changes in the intensity of extremely wet events, which is defined as the upper decile of precipitation in the wet days (cluster 1 MAM and cluster 2 JAS) during a given period (Fig. S4). Similar to the changes in wet anomalies (Figs. 7a,d), the intensity of extremely wet events shows a significant increase across the Midwest during spring, particularly over the central Midwest(e.g., Illinois, Wisconsin, Iowa, and Missouri) with more than a 2 mm day^{-1} increase. Significantly intensified wet events are also found in the southern Midwest during summer. It is notable that changes in extreme wet events are disproportionately larger than the changes in the mean precipitation.

Figure 8 shows the climatology of vertically integrated moisture flux associated with the five circulation clusters in spring and summer during 1981–2010, and its projected changes by the end of the century. During spring, cluster 1 MAM is associated with strong moisture flux from the Gulf of Mexico into the Midwest (Fig. 8a), resulting in high precipitation over this region. Such moisture flux–extreme precipitation relationships are also documented in previous studies (Zhang and Villarini 2019; Davenport and Diffenbaugh 2021). On the other hand, cluster 2 MAM shows a very small amount of moisture flux from the southern plains (Fig. 8b), corresponding to strong dry anomalies. During summer, cluster 1 JAS is associated with limited moisture flux into the Midwest (Fig. 8c), corresponding to the extremely dry conditions identified in Fig. 5. Cluster 2 JAS, which presents strong wet anomalies in the Midwest (Fig. 3), exhibits strong moisture flux from the Gulf of
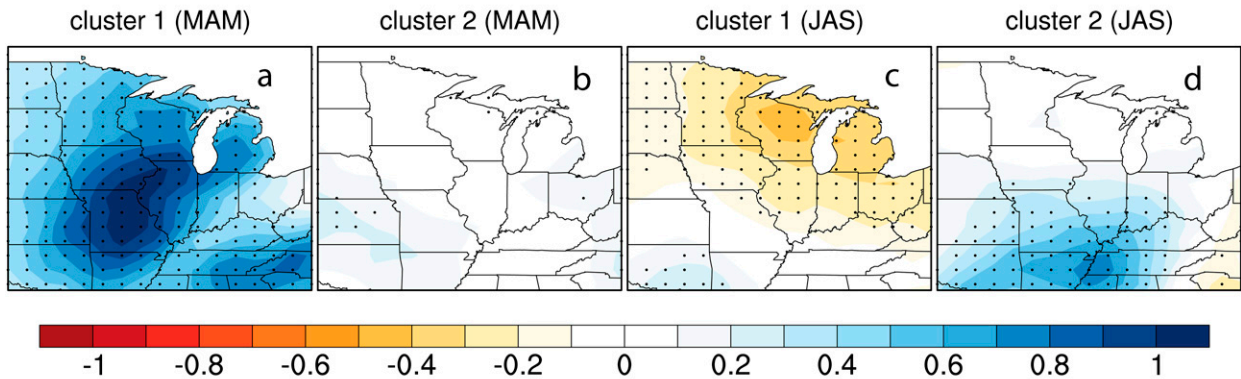
FIG. 7. Projected changes in precipitation anomalies (mm day^{-1}) associated with (a),(b) clusters 1 and 2 in spring and (c),(d) clusters 1 and 2 in summer. The changes are calculated based on the difference between the SSP370 period 2071–2100 and the historical period 1981–2010. Stippling indicates that over 75% of the ensembles of CESM2-LE agree on the sign of the change.

Mexico (Fig. 8d). By the end of the century, there is a significant increase in moisture flux into the Midwest in cluster 1 MAM (Fig. 8e). Again, this suggests that the intensity of springtime wet extremes will potentially increase. However, cluster 1 JAS does not show evident changes in moisture flux over the Midwest. Meanwhile, we note that the moisture flux tends to increase under cluster 2 in summer, preferentially leading to an increase in precipitation intensity during wet days, even though the frequency of cluster 2 is projected to decrease.

6. Mechanism of projected changes

First, we examine the anomalies of moisture budget associated with the wet and dry conditions in spring and summer (Fig. 9). Generally, the vertically integrated water budget can well resemble the precipitation anomalies but with a different magnitude. It should be noted that the anomalies of evapotranspiration are negligible (not shown), so the anomalies of $P - E$ are mostly from the precipitation anomalies. Also, all the water budget terms show opposite patterns between the wet and dry conditions (e.g., cluster 1 MAM vs cluster 2 MAM, cluster 1 JAS vs cluster 2 JAS).

Among the three terms of the vertically integrated water budget, the contribution from the thermodynamic component of vertical moisture advection is minimal, while the dynamic component plays a dominant role, suggesting the variability of precipitation is strongly associated with atmospheric circulation and convection. For instance, during the wet conditions in spring (Figs. 9a–e), the dynamic term shows evident positive moisture anomalies over the majority of the Midwest and the eastern United States (Fig. 9c), which agree with the positive precipitation anomalies (Fig. 9e). Although the horizontal
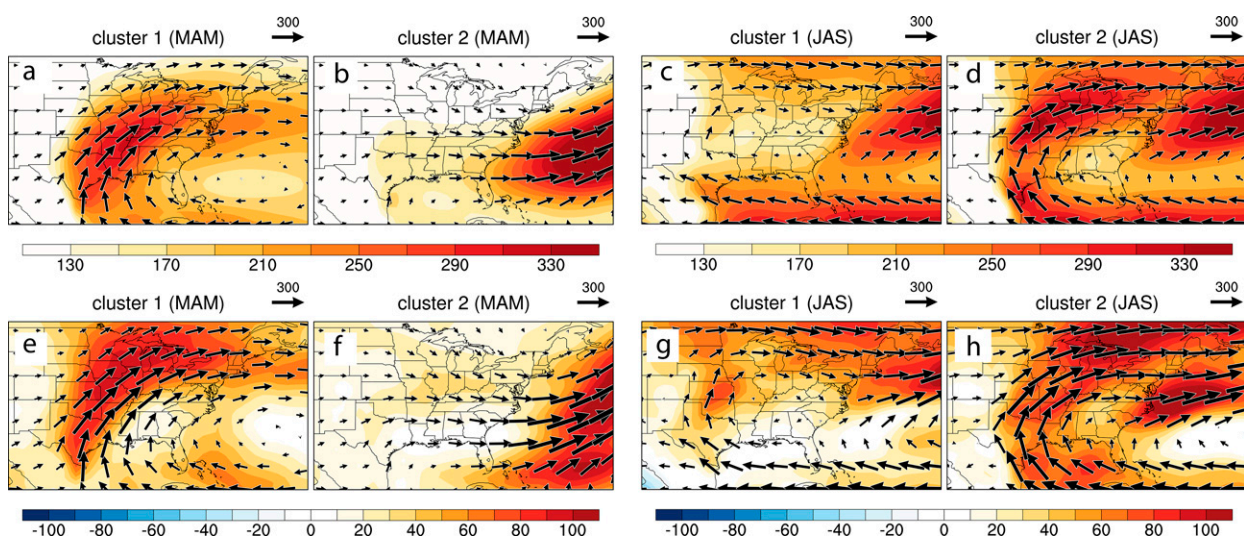

FIG. 8. Climatology of vertically integrated moisture flux (kg m^{-1} s^{-1}) associated with (a),(b) clusters 1 and 2 in spring and (c),(d) clusters 1 and 2 in summer during the period 1981–2010 and (e)–(h) the projected changes in moisture flux by 2071–2100. Arrows in all the panels show the actual magnitude and direction of moisture flux.
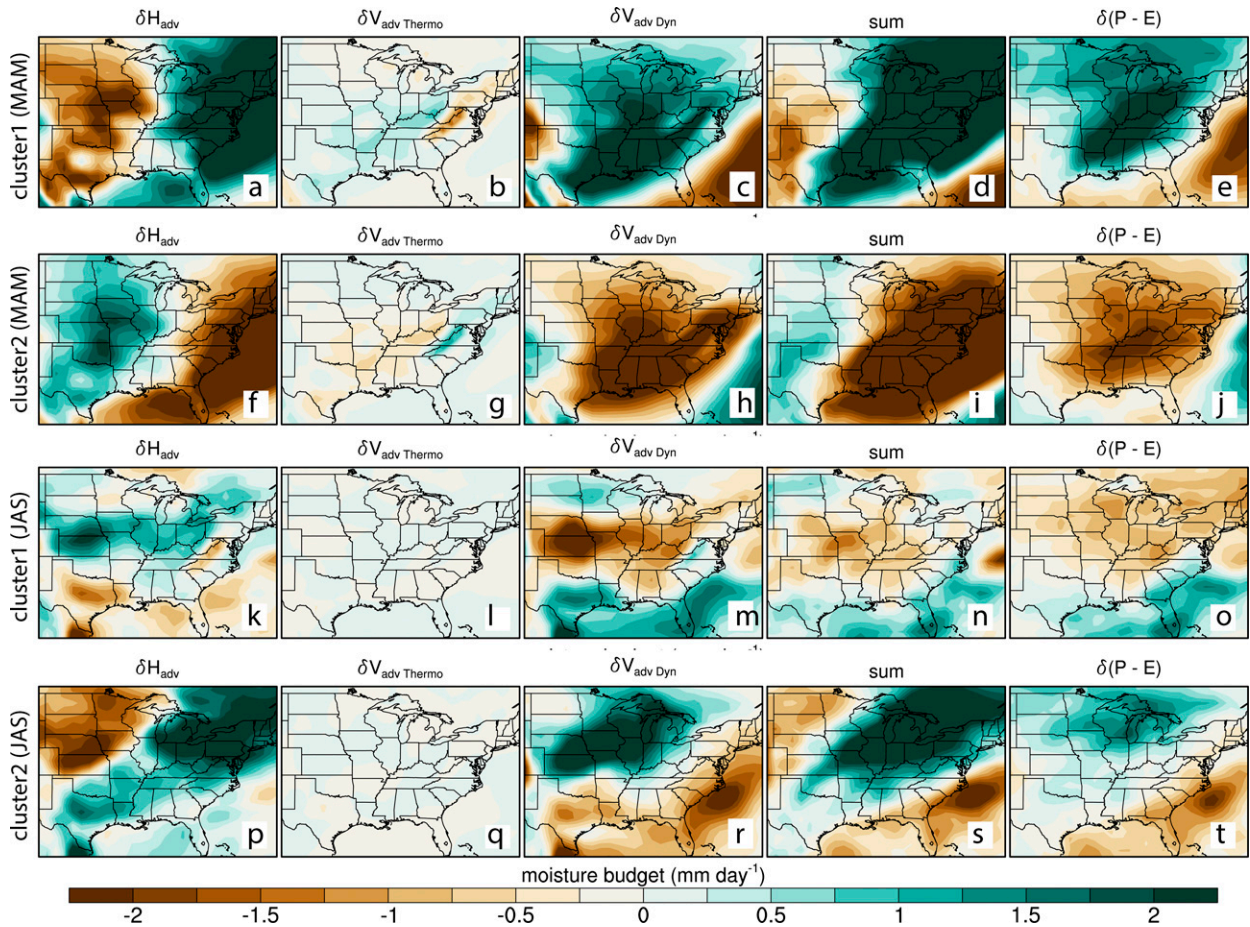
FIG. 9. Composite anomalies of (first column) horizontal moisture advection, (second column) thermodynamic and (third column) dynamic components of vertical moisture advection, (fourth column) the sum of all the terms on the right side of Eq. (5), and (fifth column) precipitation minus evaporation associated with (a)–(e) cluster 1 MAM, (f)–(j) cluster 2 MAM, (k)–(o) cluster 1 JAS, and (p)–(t) cluster 2 JAS during summer of the historical period 1981–2010.

moisture advection also shows strong anomalies, the sign of the changes and their spatial patterns do not resemble the precipitation anomalies. The dominance of dynamic effects in precipitation extremes also agrees with previous studies (such as Sudharsan et al. 2020; Tan et al. 2022).

Figure 10 shows the projected changes in moisture budget by the end of the twenty-first century. Although the seasonal total precipitation shows a significant increase in spring and a decrease in summer (not shown), changes in the term $(P - E)$ are less evident because evapotranspiration follows the changes in precipitation (increase during spring and decrease during summer over the central United States, not shown). Like the anomalies of moisture budget during the historical period, the vertically integrated water budget can well resemble the projected changes in $P - E$, and the dynamic effects play a more important role with respect to the magnitude and spatial pattern. However, the dynamic term shows an increased contribution to precipitation in most areas of the Midwest during both spring and summer. The seasonal overall increase in dynamic effects would favor the wet conditions (e.g., cluster 1 MAM), but the projected increase in dry

extremes in summer cannot be explicitly explained by the moisture budget.

Furthermore, we examine the anomalies of 500-hPa zonal wind, sea level pressure (SLP), and storm tracks during the wet and dry conditions in spring and summer, and the projected changes in their seasonal average (Fig. 11). In cluster 1 MAM, there are an evident northward shift of NAWJ and positive SLP anomalies over the western Atlantic, which strengthen the southerlies to its west and leads to intensified Great Plains low-level jet (Fig. 8). The link between large-scale circulation, synoptic patterns, and associated precipitation anomalies well agrees with the findings of Zhou et al. (2022), in which the projected increase in springtime precipitation over the Midwest is attributed to the poleward shift of the NAWJ that favors the development of cluster 1 MAM pattern and lead to more precipitation. The dry conditions (cluster 2 MAM) exhibit an opposite pattern in the anomalies of NAWJ and SLP to that in cluster 1 MAM. During the dry conditions in summer (cluster 1 JAS), the poleward shift of NAWJ and the anomalies of SLP are relatively weak. When examining the anomalies of storm tracks, the dry cluster in
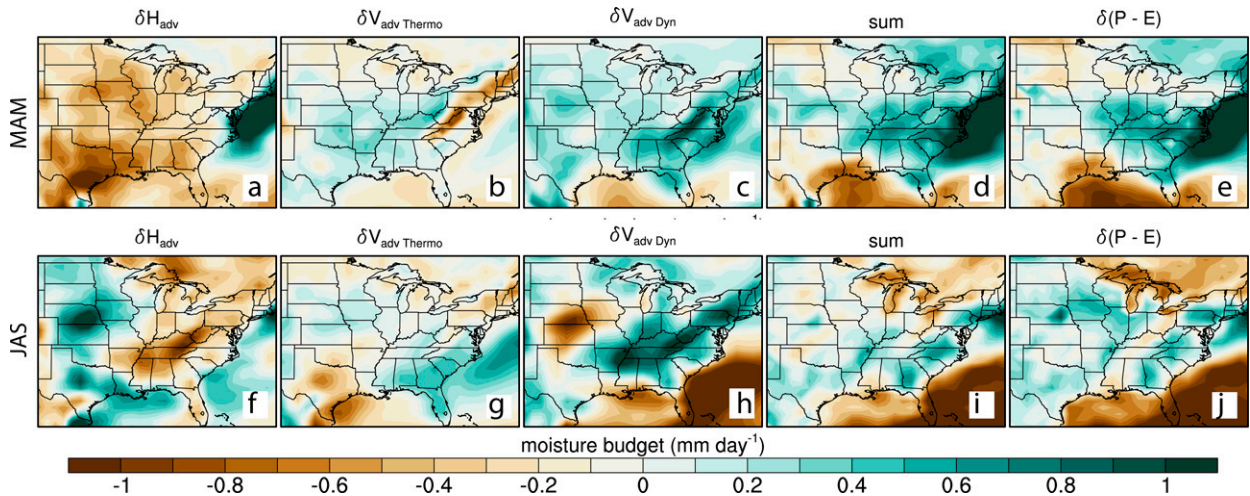
FIG. 10. Seasonal changes in (first column) horizontal moisture advection, (second column) thermodynamic and (third column) dynamic components of vertical moisture advection, (fourth column) the sum of all the terms on the right side of Eq. (5), and (fifth column) precipitation minus evaporation in (a)–(e) spring and (f)–(j) summer during the SSP370 period 2071–2100 relative to the historical period 1981–2010.

summer corresponds to evidently reduced storm tracks over the Midwest (Fig. 11n). Nevertheless, the projected changes in NAWJ, SLP, and storm tracks well resemble their anomalies in cluster 1 JAS, suggesting that future large-scale conditions would promote the dry conditions in summer.

7. Model-associated uncertainties

It should be noted that the projected changes discussed above are based on the large-ensemble experiments of CESM2. To explore the uncertainties related to the choice of climate models, we conduct the *k*-means clustering in 10 CMIP6 models (Table S1). Figure S5 shows cluster 1 of Z500 anomalies and associated precipitation anomalies in spring and summer. Similar to the CESM2-LE and reanalysis datasets, cluster 1 MAM is characterized by positive anomalies over the eastern United States and slightly negative anomalies over the western United States, and cluster 1 JAS features a high pressure system over the Great Lakes region. Consequently, the two clusters are associated with evident wet anomalies in spring and dry anomalies in summer (Fig. S6). Overall, the identified circulation patterns and associated precipitation anomalies in CMIP6 are consistent with the results based on CESM2-LE.

The frequency trends of cluster 1 in CMIP6 are shown in Fig. S7. CMIP6 models exhibit an increasing trend of cluster 1 in both summer and spring but with a smaller magnitude than CESM2-LE. Similarly, the trend in summer is slightly greater than that in spring, but there is a considerable intermodel spread in both seasons. When checking the projected changes in associated precipitation anomalies (Fig. S8), there is a good consensus that springtime wet conditions are getting more intense. Similar to the CESM2-LE results, the CMIP6 models suggest intensified dry conditions in summer over the northern Midwest.

8. Discussion and conclusions

This study reveals the key atmospheric circulation patterns that are associated with the springtime wet extremes and summertime dry extremes in the U.S. Midwest. The identified patterns are consistent with recent studies that use different approaches (e.g., Zhang and Villarini 2019; Davenport and Diffenbaugh 2021; Paxton et al. 2021). The springtime wet extremes are typically linked to baroclinic waves, which favor the development of the Great Plains low-level jet (Feng et al. 2016); the summertime dry extremes are concurrent with the development of an anomalous ridge (Ford and Labosier 2017; Wang et al. 2015). The *k*-means clustering applied to 500-hPa geopotential height anomalies can well characterize the atmospheric conditions of wet and dry extremes in the Midwest. For instance, the time series of frequency of cluster 1 JAS based on ERA5 and MERRA-2 shows high frequency in the years 1983 and 2012, which correspond to two severe drought events in the Midwest, and very low frequency in the years 1986 and 1993, which correspond to two flood disasters in the Midwest (Fig. S9). This approach is also beneficial because geopotential height itself is inherently more predictable and more skillfully represented in models (compared to precipitation which depends heavily on convective parameterization and interaction with the land surface). Therefore, this approach can potentially be used to improve the subseasonal to seasonal predictability and prediction skill of these extremes. Along these lines, one might use a model to predict the frequency of occurrence of each cluster in conjunction with the observed relationship between clusters and precipitation (i.e., downscaling), and possibly improve precipitation forecasts.

Meanwhile, we see a good agreement in the identified atmospheric patterns among reanalysis datasets, CESM2-LE, and CMIP6 simulations, but a discrepancy in the associated precipitation anomalies of each cluster among the datasets,
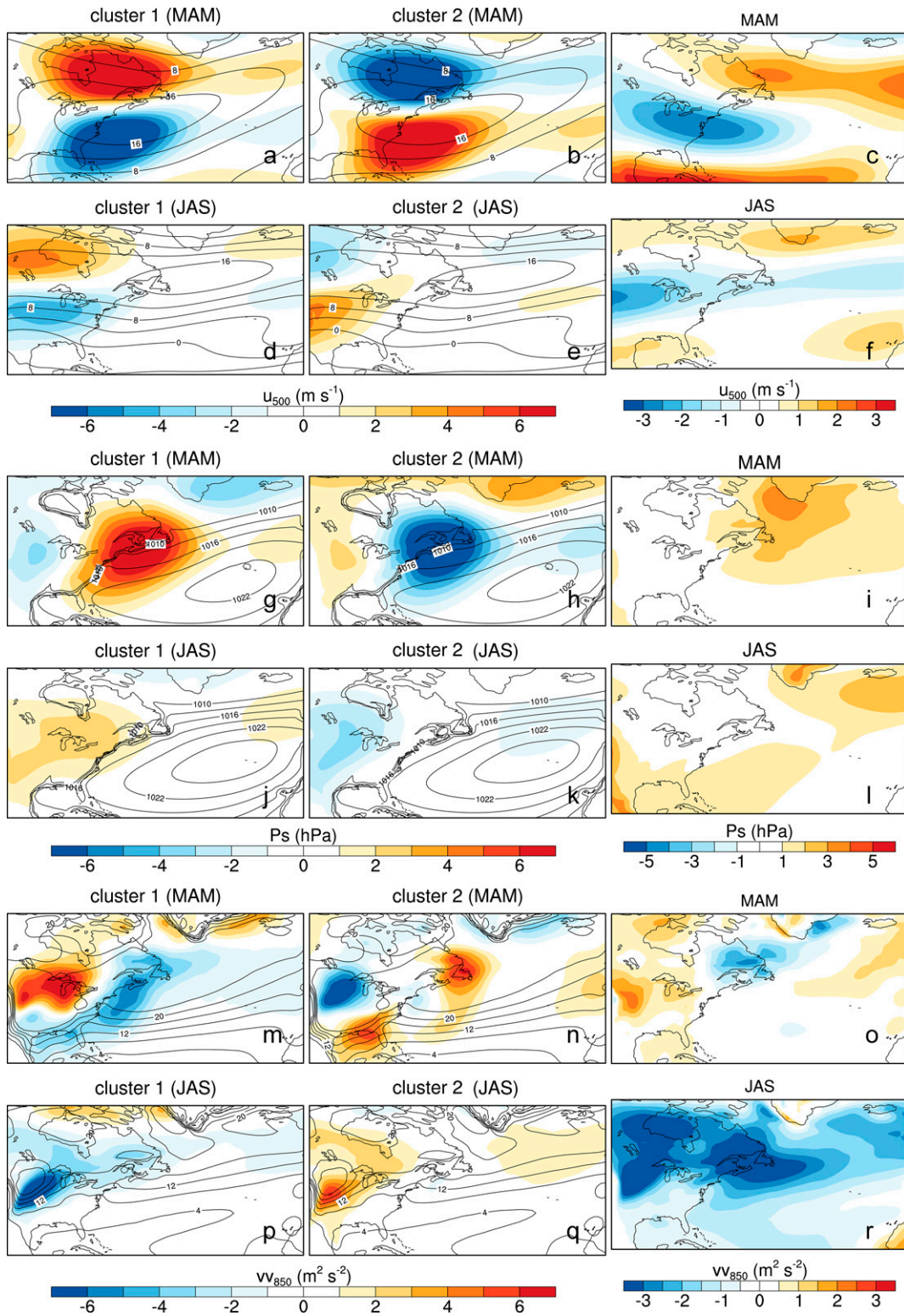
FIG. 11. Anomalies (shading) of (a)–(f) 500-hPa zonal wind, (g)–(l) sea level pressure, and (m)–(r) storm tracks in (left),(center) wet and dry clusters in spring and summer and (right) the projected changes in seasonal average during the SSP370 period 2071–2100 relative to the historical period 1981–2010. Contours in the maps show the seasonal climatology during the historical period 1981–2010.

suggesting the uncertainty of representing precipitation processes in state-of-the-art global climate models (GCMs). Because land–atmosphere interactions (such as soil moisture–rainfall feedback) can be an important mechanism for the precipitation processes of the U.S. Midwest during the spring or summer (Pal and Eltahir 2001; Sun and Liang 2020), the discrepancy in the associated precipitation anomalies can also be attributed to the uncertainties related to land–atmosphere coupling in different climate models (Sippel et al. 2017; Dong et al. 2020). Nevertheless, our study suggests robust changes in large-scale circulation patterns among the ensemble simulations, providing useful insight into the projections of hydroclimatic extremes.

Our results show that the increased wet extremes in spring and dry extremes in summer can be attributed to significantly more frequent occurrences of the associated atmospheric regimes. The mechanism analysis further reveals that the anomalies and trends in precipitation extremes are mainly associated with the dynamic component of atmospheric circulation, and the atmospheric regimes can be linked to the changes in NAWJ, SLP, and Great Plains low-level jet during the springtime wet extremes, and to the suppressed storm tracks during the summertime dry extremes, thus proving a more complete picture of the mechanism of projected hydroclimatic extremes in the Midwest. The trend of extreme precipitation and associated large-scale environment in spring is also documented in the observation-based study (Feng et al. 2016), which suggests that the observed springtime extreme precipitation can be explained by increased frequency and intensity of long-lasting mesoscale convective systems. This agreement indicates that the analysis of atmospheric regimes can provide insight into the physical mechanisms of regional precipitation extremes despite the poor representation of mesoscale processes in current GCMs. The projected increase in summer drought also agrees with the historical analysis (Wang et al. 2015), which reveals that there is persistent subseasonal rainfall reduction from June to July since 1979, and the enhanced summer drought can be associated with tropospheric subsidence, enhanced evaporative fraction, and elevated planetary boundary layer height. Although our results do not show the summer precipitation deficit will be intensified in large areas, the associated atmospheric conditions (such as elevated temperature and vapor pressure deficit; Zhao and Dai 2022) and land–atmosphere interactions (such as soil moisture and vegetation feedback; Zhou et al. 2019; Zhang et al. 2021) can also intensify surface drying.

Both CESM2-LE and CMIP6 suggest increased wet spring and dry summer, which pose a significant threat to water management and agricultural production in the Midwest. The increased frequency and intensity of wet extremes will raise flood risks and challenge drainage systems in urban areas (Yazdanfar and Sharma 2015). Meanwhile, excess rainfall in spring can cause planting delay and shortened growing season (Shirzaei et al. 2021), and lead to nutrient loss and soil erosion (Rao and Li 2003; Kleinman et al. 2006). Furthermore, the combined effects of wet spring and dry summer will be of great concern for Midwest producers, which have devastating impacts on crop production (Grady et al. 2021).

Data availability statement. The CESM2-LE data are available at https://www.cesm.ucar.edu/projects/community-projects/LENS2/data-sets.html. CMIP6 output is available from public repositories, https://esgf-node.llnl.gov/projects/cmip6/. The ERA5 dataset is available on the Climate data store (CDS) https://cds.climate.copernicus.eu/. The MERRA-2 dataset is downloaded from https://disc.gsfc.nasa.gov/datasets?project=MERRA-2. NCL codes for data analysis can be found at https://doi.org/10.5281/zenodo.7301882.

REFERENCES

Agel, L., and M. Barlow, 2020: How well do CMIP6 historical runs match observed northeast U.S. precipitation and extreme precipitation–related circulation? *J. Climate*, **33**, 9835–9848, https://doi.org/10.1175/JCLI-D-19-1025.1.

——, ——, C. Skinner, F. Colby, and J. Cohen, 2021: Four distinct northeast US heat wave circulation patterns and associated mechanisms, trends, and electric usage. *npj Climate Atmos. Sci.*, **4**, 31, https://doi.org/10.1038/s41612-021-00186-7.

Akinsanola, A. A., G. J. Kooperman, K. A. Reed, A. G. Pendergrass, and W. M. Hannah, 2020: Projected changes in seasonal precipitation extremes over the United States in CMIP6 simulations. *Environ. Res. Lett.*, **15**, 104078, https://doi.org/10.1088/1748-9326/abb397.

Cao, F., T. Gao, L. Dan, Z. Ma, X. Chen, L. Zou, and L. Zhang, 2019: Synoptic-scale atmospheric circulation anomalies associated with summertime daily precipitation extremes in the middle–lower reaches of the Yangtze River basin. *Climate Dyn.*, **53**, 3109–3129, https://doi.org/10.1007/s00382-019-04687-3.

Chen, L., and T. W. Ford, 2021: Effects of 0.5°C less global warming on climate extremes in the contiguous United States. *Climate Dyn.*, **57**, 303–319, https://doi.org/10.1007/s00382-021-05717-9.

——, and ——, 2023: Future changes in the transitions of monthly-to-seasonal precipitation extremes over the Midwest in Coupled Model Intercomparison Project Phase 6 models. *Int. J. Climatol.*, **43**, 255–274, https://doi.org/10.1002/joc.7756.

Chen, W., D.-B. Jiang, X.-M. Lang, and Z.-P. Tian, 2021: Understanding the cold biases of CMIP5 models over China with weather regimes. *Adv. Climate Change Res.*, **12**, 373–383, https://doi.org/10.1016/j.accre.2021.05.002.

Chou, C., and C.-W. Lan, 2012: Changes in the annual range of precipitation under global warming. *J. Climate*, **25**, 222–235, https://doi.org/10.1175/JCLI-D-11-00097.1.

Cook, B. I., J. S. Mankin, K. Marvel, A. P. Williams, J. E. Smerdon, and K. J. Anchukaitis, 2020: Twenty-first century drought projections in the CMIP6 forcing scenarios. *Earth's Future*, **8**, e2019EF001461, https://doi.org/10.1029/2019EF001461.

Danabasoglu, G., and Coauthors, 2020: The Community Earth System Model version 2 (CESM2). *J. Adv. Model. Earth Syst.*, **12**, e2019MS001916, https://doi.org/10.1029/2019MS001916.

Davenport, F. V., and N. S. Diffenbaugh, 2021: Using machine learning to analyze physical causes of climate change: A case study of U.S. Midwest extreme precipitation. *Geophys. Res. Lett.*, **48**, e2021GL093787, https://doi.org/10.1029/2021GL093787.

Dong, J., P. A. Dirmeyer, F. Lei, M. C. Anderson, T. R. H. Holmes, C. Hain, and W. T. Crow, 2020: Soil evaporation stress determines soil moisture-evapotranspiration coupling strength in land surface modeling. *Geophys. Res. Lett.*, **47**, e2020GL090391, https://doi.org/10.1029/2020GL090391.

Feng, X., B. Huang, G. Tintera, and B. Chen, 2019: An examination of the Northern Hemisphere mid-latitude storm track interannual variability simulated by climate models—Sensitivity to model resolution and coupling. *Climate Dyn.*, **52**, 4247–4268, https://doi.org/10.1007/s00382-018-4378-x.

Feng, Z., L. R. Leung, S. Hagos, R. A. Houze, C. D. Burleyson, and K. Balaguru, 2016: More frequent intense and long-lived storms dominate the springtime trend in central US rainfall. *Nat. Commun.*, **7**, 13429, https://doi.org/10.1038/ncomms13429.

Ford, T. W., and C. F. Labosier, 2017: Meteorological conditions associated with the onset of flash drought in the eastern United States. *Agric. For. Meteor.*, **247**, 414–423, https://doi.org/10.1016/j.agrformet.2017.08.031.

Frankcombe, L. M., M. H. England, J. B. Kajtar, M. E. Mann, and B. A. Steinman, 2018: On the choice of ensemble mean for estimating the forced signal in the presence of internal variability. *J. Climate*, **31**, 5681–5693, https://doi.org/10.1175/JCLI-D-17-0662.1.

Gelaro, R., and Coauthors, 2017: The Modern-Era Retrospective Analysis For Research And Applications, version 2 (MERRA-2). *J. Climate*, **30**, 5419–5454, https://doi.org/10.1175/JCLI-D-16-0758.1.

Gibson, P. B., A. J. Pitman, R. Lorenz, and S. E. Perkins-Kirkpatrick, 2017: The role of circulation and land surface conditions in current and future Australian heat waves. *J. Climate*, **30**, 9933–9948, https://doi.org/10.1175/JCLI-D-17-0265.1.

Grady, K. A., L. Chen, and T. W. Ford, 2021: Projected changes to spring and summer precipitation in the midwestern United States. *Front. Water*, **3**, 780333, https://doi.org/10.3389/frwa.2021.780333.

Hartigan, J. A., and M. A. Wong, 1979: Algorithm AS136: A K-means clustering algorithm. *Appl. Stat.*, **28**, 100–108, https://doi.org/10.2307/2346830.

Hernandez, M., and L. Chen, 2022: Future land precipitation changes over the North American monsoon region using CMIP5 and CMIP6 simulations. *J. Geophys. Res. Atmos.*, **127**, e2021JD035911, https://doi.org/10.1029/2021JD035911.

Hersbach, H., and Coauthors, 2020: The ERA5 global reanalysis. *Quart. J. Roy. Meteor. Soc.*, **146**, 1999–2049, https://doi.org/10.1002/qj.3803.

Hoerling, M., J. Eischeid, A. Kumar, R. Leung, A. Mariotti, K. Mo, S. Schubert, and R. Seager, 2014: Causes and predictability of the 2012 Great Plains drought. *Bull. Amer. Meteor. Soc.*, **95**, 269–282, https://doi.org/10.1175/BAMS-D-13-00055.1.

Jézéquel, A., P. Yiou, and S. Radanovics, 2018: Role of circulation in European heatwaves using flow analogues. *Climate Dyn.*, **50**, 1145–1159, https://doi.org/10.1007/s00382-017-3667-0.

Kay, J. E., and Coauthors, 2015: The Community Earth System Model (CESM) large ensemble project: A community resource for studying climate change in the presence of internal climate variability. *Bull. Amer. Meteor. Soc.*, **96**, 1333–1349, https://doi.org/10.1175/BAMS-D-13-00255.1.

Kleinman, P. J. A., M. S. Srinivasan, C. J. Dell, J. P. Schmidt, A. N. Sharpley, and R. B. Bryant, 2006: Role of rainfall intensity and hydrology in nutrient transport via surface runoff. *J. Environ. Qual.*, **35**, 1248–1259, https://doi.org/10.2134/jeq2006.0015.

Kunkel, K. E., T. R. Karl, M. F. Squires, X. Yin, S. T. Stegall, and D. R. Easterling, 2020: Precipitation extremes: Trends and relationships with average precipitation and precipitable water in the contiguous United States. *J. Appl. Meteor. Climatol.*, **59**, 125–142, https://doi.org/10.1175/JAMC-D-19-0185.1.

Li, M., Q. Sun, M. A. Lovino, S. Ali, M. Islam, T. Li, C. Li, and Z. Jiang, 2022: Non-uniform changes in different daily precipitation events in the contiguous United States. *Wea. Climate Extremes*, **35**, 100417, https://doi.org/10.1016/j.wace.2022.100417.

Li, Y., K. Guan, G. D. Schnitkey, E. DeLucia, and B. Peng, 2019: Excessive rainfall leads to maize yield loss of a comparable magnitude to extreme drought in the United States. *Global Change Biol.*, **25**, 2325–2337, https://doi.org/10.1111/gcb.14628.

Loecke, T. D., A. J. Burgin, D. A. Riveros-Iregui, A. S. Ward, S. A. Thomas, C. A. Davis, and M. A. St. Clair, 2017: Weather whiplash in agricultural regions drives deterioration of water quality. *Biogeochemistry*, **133**, 7–15, https://doi.org/10.1007/s10533-017-0315-z.

Lutsko, N. J., J. W. Baldwin, and T. W. Cronin, 2019: The impact of large-scale orography on Northern Hemisphere winter synoptic temperature variability. *J. Climate*, **32**, 5799–5814, https://doi.org/10.1175/JCLI-D-19-0129.1.

Magee, M. R., and Coauthors, 2019: Scientific advances and adaptation strategies for Wisconsin lakes facing climate change. *Lake Reservoir Manage.*, **35**, 364–381, https://doi.org/10.1080/10402381.2019.1622612.

Mastrantonas, N., P. Herrera-Lormendez, L. Magnusson, F. Pappenberger, and J. Matschullat, 2021: Extreme precipitation events in the Mediterranean: Spatiotemporal characteristics and connection to large-scale atmospheric flow patterns. *Int. J. Climatol.*, **41**, 2710–2728, https://doi.org/10.1002/joc.6985.

Milinski, S., N. Maher, and D. Olonscheck, 2020: How large does a large ensemble need to be? *Earth Syst. Dyn.*, **11**, 885–901, https://doi.org/10.5194/esd-11-885-2020.

Moore, T. L., J. S. Gulliver, L. Stack, and M. H. Simpson, 2016: Stormwater management and climate change: Vulnerability and capacity for adaptation in urban and suburban contexts. *Climatic Change*, **138**, 491–504, https://doi.org/10.1007/s10584-016-1766-2.

NOAA, 2022: U.S. billion-dollar weather and climate disasters. National Centers for Environmental Information, https://doi.org/10.25921/stkw-7w73.

O'Gorman, P. A., and T. Schneider, 2009: The physical basis for increases in precipitation extremes in simulations of 21st-century climate change. *Proc. Natl. Acad. Sci. USA*, **106**, 14773–14777, https://doi.org/10.1073/pnas.0907610106.

Pal, J. S., and E. A. B. Eltahir, 2001: Pathways relating soil moisture conditions to future summer rainfall within a model of the land–atmosphere system. *J. Climate*, **14**, 1227–1242, https://doi.org/10.1175/1520-0442(2001)014<1227:PRSMCT>2.0.CO;2.

Paxton, A., J. T. Schoof, T. W. Ford, and J. W. F. Remo, 2021: Extreme precipitation in the Great Lakes region: Trend estimation and relation with large-scale circulation and humidity. *Front. Water*, **3**, 782847, https://doi.org/10.3389/frwa.2021.782847.

Rao, R., and Y. Li, 2003: Management of flooding effects on growth of vegetable and selected field crops. *HortTechnology*, **13**, 610–616, https://doi.org/10.21273/HORTTECH.13.4.0610.

Rodgers, K. B., and Coauthors, 2021: Ubiquity of human-induced changes in climate variability. *Earth Syst. Dyn.*, **12**, 1393–1411, https://doi.org/10.5194/esd-12-1393-2021.

Schubert, S. D., M. J. Suarez, P. J. Pegion, R. D. Koster, and J. T. Bacmeister, 2004: Causes of long-term drought in the U.S. Great Plains. *J. Climate*, **17**, 485–503, https://doi.org/10.1175/1520-0442(2004)017<0485:COLDIT>2.0.CO;2.

Seager, R., and G. A. Vecchi, 2010: Greenhouse warming and the 21st century hydroclimate of southwestern North America. *Proc. Natl. Acad. Sci. USA*, **107**, 21277–21282, https://doi.org/10.1073/pnas.0910856107.

Shirzaei, M., and Coauthors, 2021: Persistent impact of spring floods on crop loss in U.S. Midwest. *Wea. Climate Extremes*, **34**, 100392, https://doi.org/10.1016/j.wace.2021.100392.

Sippel, S., J. Zscheischler, M. D. Mahecha, R. Orth, M. Reichstein, M. Vogel, and S. I. Seneviratne, 2017: Refining multi-model projections of temperature extremes by evaluation against land–atmosphere coupling diagnostics. *Earth Syst. Dyn.*, **8**, 387–403, https://doi.org/10.5194/esd-8-387-2017.

Straus, D. M., 2019: Clustering techniques in climate analysis. *Oxford Research Encyclopedia of Climate Science*, Oxford University Press, https://doi.org/10.1093/acrefore/9780190228620.013.711.

Sudharsan, N., S. Karmakar, H. J. Fowler, and V. Hari, 2020: Large-scale dynamics have greater role than thermodynamics in driving precipitation extremes over India. *Climate Dyn.*, **55**, 2603–2614, https://doi.org/10.1007/s00382-020-05410-3.

Sun, C., and X.-Z. Liang, 2020: Improving US extreme precipitation simulation: Dependence on cumulus parameterization and underlying mechanism. *Climate Dyn.*, **55**, 1325–1352, https://doi.org/10.1007/s00382-020-05328-w.

Swanston, C., and Coauthors, 2018: Vulnerability of forests of the Midwest and Northeast United States to climate change.

Climatic Change, **146**, 103–116, https://doi.org/10.1007/s10584-017-2065-2.

Tan, Y., S. Yang, F. Zwiers, Z. Wang, and Q. Sun, 2022: Moisture budget analysis of extreme precipitation associated with different types of atmospheric rivers over western North America. *Climate Dyn.*, **58**, 793–809, https://doi.org/10.1007/s00382-021-05933-3.

Thomas, C., A. Voulgarakis, G. Lim, J. Haigh, and P. Nowack, 2021: An unsupervised learning approach to identifying blocking events: The case of European summer. *Wea. Climate Dyn.*, **2**, 581–608, https://doi.org/10.5194/wcd-2-581-2021.

Urban, D. W., M. J. Roberts, W. Schlenker, and D. B. Lobell, 2015: The effects of extremely wet planting conditions on maize and soybean yields. *Climatic Change*, **130**, 247–260, https://doi.org/10.1007/s10584-015-1362-x.

Wang, S.-Y. S., and Coauthors, 2015: An intensified seasonal transition in the central U.S. that enhances summer drought. *J. Geophys. Res. Atmos.*, **120**, 8804–8816, https://doi.org/10.1002/2014JD023013.

Westcott, N. E., S. E. Hollinger, and K. E. Kunkel, 2005: Use of real-time multisensor data to assess the relationship of normalized corn yield with monthly rainfall and heat stress across the central United States. *J. Appl. Meteor.*, **44**, 1667–1676, https://doi.org/10.1175/JAM2303.1.

Yazdanfar, Z., and A. Sharma, 2015: Urban drainage system planning and design—Challenges with climate change and urbanization: A review. *Water Sci. Technol.*, **72**, 165–179, https://doi.org/10.2166/wst.2015.207.

Zhang, W., and G. Villarini, 2019: On the weather types that shape the precipitation patterns across the U.S. Midwest. *Climate Dyn.*, **53**, 4217–4232, https://doi.org/10.1007/s00382-019-04783-4.

Zhang, Y., T. F. Keenan, and S. Zhou, 2021: Exacerbated drought impacts on global ecosystems due to structural overshoot. *Nat. Ecol. Evol.*, **5**, 1490–1498, https://doi.org/10.1038/s41559-021-01551-8.

Zhao, T., and A. Dai, 2022: CMIP6 model-projected hydroclimatic and drought changes and their causes in the twenty-first century. *J. Climate*, **35**, 897–921, https://doi.org/10.1175/JCLI-D-21-0442.1.

Zhou, S., and Coauthors, 2019: Land–atmosphere feedbacks exacerbate concurrent soil drought and atmospheric aridity. *Proc. Natl. Acad. Sci. USA*, **116**, 18848–18853, https://doi.org/10.1073/pnas.1904955116.

Zhou, W., L. R. Leung, F. Song, and J. Lu, 2021: Future changes in the Great Plains low-level jet governed by seasonally dependent pattern changes in the North Atlantic subtropical high. *Geophys. Res. Lett.*, **48**, e2020GL090356, https://doi.org/10.1029/2020GL090356.

——, ——, and J. Lu, 2022: Seasonally dependent future changes in the U.S. Midwest hydroclimate and extremes. *J. Climate*, **35**, 17–27, https://doi.org/10.1175/JCLI-D-21-0012.1.